**ORIGINAL PAPER**

Electrooxidation of 1-propanol on the mixture of nanoparticles of Pt and RuO$_2$

Milica Spasojević[1] · Lenka Ribić-Zelenović[2] · Miroslav Spasojević[2]

Abstract

The catalyst composed of a mixture of nanocrystals of metallic Pt and rutile RuO$_2$ was prepared by a thermal procedure on a titanium substrate. An effect of the mixture composition on its microstructure, surface properties, and catalytic activity for an electrooxidation of 1-propanol in an alkaline environment was examined. The relation between the microstructure of the Pt/RuO$_2$ catalyst and its catalytic activity was determined. It was found that the increase in the RuO$_2$ content resulted in the increase in the catalytic activity, which reached its maximum value and then decreased. The catalytic effect was caused by the bifunctional mechanism of the catalyst Pt/RuO$_2$. Ru-OH species were formed on Ru atoms of RuO$_2$ nanocrystals at more negative potentials than on Pt. These oxy species oxidized firmly adsorbed intermediates propionyl, CO$_{ad}$, C$_2$H$_{yad}$, and CH$_{ad}$ and, thus, released Pt atoms for the adsorption and dehydrogenation of the subsequent molecules of 1-propanol.

Graphic abstract
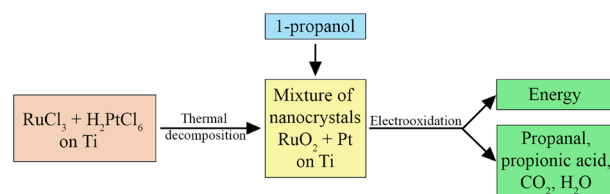
Keywords Nanostructures · Fuel cell · Bifunctional mechanism · Catalysts · Cyclic voltammetry · Electrochemistry

Introduction

Development of renewable energies has been an aim of many research groups in the last couple of decades. Fuel cells, in particular direct liquid-feed fuel cells, have been a main focus of researches conducted in this field. The liquid fuel cells based on alcohols have shown a great potential as renewable power sources. The liquid fuel cells have many advantages over the gaseous cells, such as a high theoretical energy density (~ 9 kWh kg^{-1}), easy handling, storage, transportation, and distribution [1]. Direct alcohol fuel cells (DAFCs) have shown to be promising power sources for portable electronic devices (mobile phones, laptop computers, digital cameras, etc.) [2, 3]. Although methanol is the mostly applied and studied alcohol for DAFCs, it is not very suitable for fuel cells due to its relative toxicity and tendency to the crossover phenomena, which slows the electrooxidation rate and affects the cathode performance. Therefore, the research has been focused on finding an adequate alternative to methanol. As less toxic alcohol, propanol is a promising substitute for methanol. Lately, many research groups have been working on development of a catalyst suitable for electrooxidation of propanol [1, 4–6].

The complete oxidation of propanol to carbon dioxide involves the transfer of 18 electrons:

✉ Milica Spasojević
smilica84@gmail.com

1 Innovation Center of Faculty of Chemistry, University of Belgrade, Belgrade, Serbia

2 Joint Laboratory for Advanced Materials of Serbian Academy of Science and Arts, Section for Amorphous Systems, Faculty of Technical Sciences, University of Kragujevac, Čačak, Serbia

$$C_3H_7OH + 5H_2O \rightarrow 3CO_2 + 18H^+ + 18e. \tag{1}$$
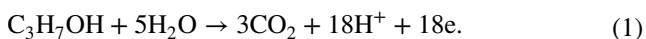
The oxidation of ethanol, methanol, and hydrogen is followed by the exchange of 12, 6, and 2 electrons, respectively. Large number of exchanged electrons involved in the oxidation of higher alcohols represents the advantage of fuel cells with these alcohols over the fuel cells with lower alcohols. Moreover, under the standard conditions, the specific energy of the direct propanol fuel cell is greater than that of ethanol and methanol fuel cells. The standard electrode potentials of the propanol oxidation and H_2 reaction are very similar [1]. The electrooxidation of 1-propanol is an incomplete reaction. A main product of the 1-propanol oxidation where 2-electron transfer occurs is propanal. Also, the oxidation of 1-propanol results in the formation of small amounts of both propionic acid and CO_2 [7–9]. Propanal can be considered as an active intermediate, since it can react further until CO_{ad}, CO_2, and adsorbed propionate formation. The oxidation of 1-propanol starts with the adsorption at Pt atoms. Subsequently, adsorbed propanol is dehydrogenized to propanal and propionyl. A portion of formed propanal transfers to solution, whereas another portion dehydrogenizes to propionyl. Propionyl is also a result of the dissociative adsorption of dissolved propanal [7–9]. Adsorbed propionyl is decomposed by splitting the C–C bond between the first and second carbon atom, which leads to the formation of adsorbed CO_{ad}, and intermediates C_2H_y and C_2H_zO [7–10]. These intermediates can be reductively desorbed at the lowest potentials, stably adsorbed at intermediate potentials and slowly decomposed to CO_{ad} at higher potentials, leaving adsorbed CH_x as the most likely fragment. At relatively high potentials, the intermediates CO_{ad}, C_2H_y, C_2H_zO, CH_x oxidize to CO_2 [7–9]. Combined and simultaneous electrochemical, in situ ATR-FT-IRs and online DEMS measurements have confirmed the presence of the intermediates: linearly CO_{Lad}, multiply CO_{Mad}, propionyl$_{ad}$, and low concentrations of bridge-bonded adsorbed propionate. Based on the number of electrons exchanged in the oxidation of firmly adsorbed species, Schnaidt et al. [7] have concluded that the firmly bound intermediates C_2H_y and CH_x are located on the Pt surface. These firmly bound intermediates block the surface Pt atoms and, thus, disable the occurrence of the adsorption and dehydrogenation of new molecules of 1-propanol. Therefore, Pt has a low activity for the electrooxidation of 1-propanol. However, the kinetics of the electrooxidation reaction has been considerably improved in the alkaline environment [11–17]. The oxidation reaction is enhanced by the OH$^-$ ions from the electrolyte. The reaction intermediates cause the electrode poisoning, which probably occurs less in the alkaline media as a consequence of reduced formation of poisoning species, resulting from the presence of the hydroxide ions [11–18].

However, the alkaline medium causes the carbonation of the alkaline electrolyte in DAFCs, and thus, prevents its use for this purpose. This obstacle has been overcome by using membranes [19–21].

The electrooxidation of 1-propanol has been mostly studied at Pt [7, 11, 12, 18–25], Pd [11, 12, 26, 27], Au [12, 28], and their alloys [14, 19, 23, 25, 29–32]. The catalytic effect of the alloys has been associated with a bifunctional mechanism and electronic effect [14, 25, 29, 33–43]. When concerning the bifunctional mechanism, the oxy species are formed at more negative potentials on alloying atoms (Ru, Sn, Bi, etc.) than on Pt atoms. The oxy species oxidize intermediates, firmly bound to the adjacent Pt atoms. The oxidized intermediates leave and, thus, release the surface, allowing for Pt atoms to adsorb and dehydrogenate subsequent simple organic molecules [14, 25, 29, 33–40]. In the electronic effect, the d-band center of Pt in the alloy shifts away from the Fermi level [25, 40–42]. As a consequence, the adsorption of the poisoning species is suppressed and thus, the poisoning effect. An effect of morphology and the size of nanoparticles on their catalytic activity in the oxidation of simple organic molecules has been examined [1, 23]. Several research groups have studied the catalytic activity of the Pt/Ru and Pt/RuO$_2$ catalysts in the electrooxidation of simple organic molecules [23, 33–47]. The good catalytic effect of the examined alloys has been attributed to both the bifunctional mechanism and electronic effect. The bifunctional mechanism has shown to be dominant [23, 33–47].

The goal of this research was to examine the catalytic activity of the catalysts, consisting of nanocrystals of both Pt and RuO$_2$, in the electrooxidation of 1-propanol. We opted for the RuO$_2$ containing catalyst because (a) the catalytic effect of this thermally prepared catalyst in the electrooxidation of 1-propanol has not been tested; (b) RuO$_2$ is expected to be more resistant to corrosion than metallic Ru in the oxidation of 1-propanol. RuO$_2$ has already proven to be less sensitive to corrosion in the chlorine–alkaline and chlorate electrolysis [48, 49]; (c) the adsorption energies of OH species on Ru atoms of RuO$_2$ and Ru atoms of the Pt/Ru alloy are distinct [50, 51]; (d) the Pt nanocrystals consist of adequate assemblies of Pt atoms, that provide the adsorption and dehydrogenation of 1-propanol molecules [36–40]; (e) a satisfactory number of Pt–Ru pairs, responsible for an adequate occurring of the bifunctional mechanism, are located at the contact edge between the RuO$_2$ and Pt nanocrystals; and (f) the surface diffusion of intermediates adsorbed on Pt is considered as a rapid process [52].

Results and discussion

The chemical composition and microstructure of the thermally synthetized Pt/RuO$_2$ coatings affect their catalytic activity in the reaction of electrooxidation of 1-propanol. To determine the correlation between the microstructure and catalytic activity, basic characteristics of the microstructure are provided in this paper. The effect of the chemical composition of the Pt/RuO$_2$ catalysts on their microstructure has been elaborated in details in our previous work [36].

Dependence of the Pt and RuO$_2$ contents, relative surface area, and electrochemically active surface area of the coatings on the nominal coatings composition is presented in Fig. 1. The diagrams show that the Pt content in the coating is slightly lower than the nominal content, whereas the RuO$_2$ content is somewhat higher than nominal. Difference is more pronounced in the coating with the higher Pt content [36]. The obtained discrepancies between the nominal and real contents of the coatings are comparable to those reported in literature [53–55].

The relative geometric surface area of Pt ($A_s(\text{Pt}) = \frac{Q(\text{H})_{\text{Pt/RuO}_2}}{Q(\text{H})_{\text{Pt}}}$) and the electrochemically active surface area of Pt ($A(\text{Pt}) = \frac{Q(\text{H})_{\text{Pt–RuO}_2}}{240m(\text{Pt})}$) are determined from cyclic voltammograms, recorded in the acidic solution (0.5 mol dm^{-3} H$_2$SO$_4$) [36]. The decrease in the Pt content results in the decline of the relative geometric surface area. This decrease is slower in the concentration region from 100 to 60 mol% Pt than in the region from 60 to 0.0 mol% Pt. With increasing the Pt content up to 60 mol%, the electrochemically active surface area also increases. However, the increase in the Pt content above 60 mol% decreases the electrochemically active surface area. Similar results with more pronounced changes are reported in literature [53, 56]. In this
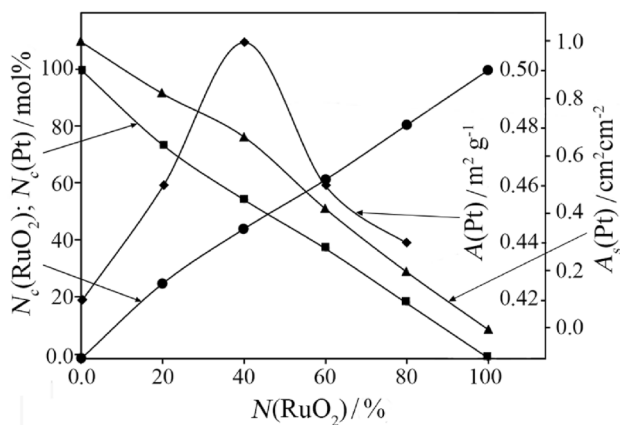
paper, changes of the electrochemically active surface area are less conspicuous since the coatings were obtained in the thermal process, which allows for substantially greater sintering [53]. Therefore, the surface roughness of these coatings alters to lesser extent with variations in the chemical composition of the coating.

The coating composition also affects the phase structure and size of crystalline grains [36]. The coatings are composed of the mixture of nanocrystals of metallic Pt and nanocrystals of rutile RuO$_2$, as shown by the XRD analysis (Fig. 2). With increasing the RuO$_2$ content in the coating, the mean size of RuO$_2$ nanocrystals increases; whereas, the mean size of Pt nanocrystals decreases (Fig. 3). The lattice parameters of the Pt and RuO$_2$ nanocrystals inconsiderably vary from the lattice parameters of pure metallic Pt and rutile RuO$_2$. This may be a consequence of inclusion of small quantities of residual chlorine or a presence
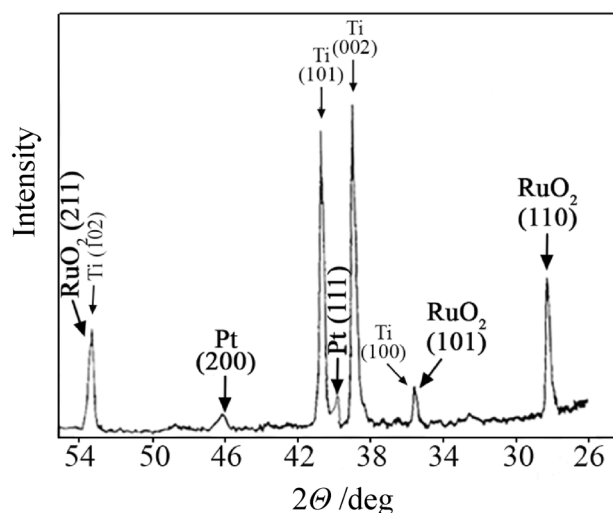

Fig. 2 X-ray diffraction pattern of the coating 60 mol% Pt, 40 mol% RuO$_2$ on the Ti substrate

Fig. 1 The content of filled square: Pt ($N_c(\text{Pt})$), filled circle: RuO$_2$ ($N_c(\text{RuO}_2)$), filled triangle: relative geometric surface area of Pt ($A_s(\text{Pt})$), and filled diamond: electrochemically active surface area ($A(\text{Pt})$) as a function of the nominal coating composition ($N(\text{RuO}_2)$)
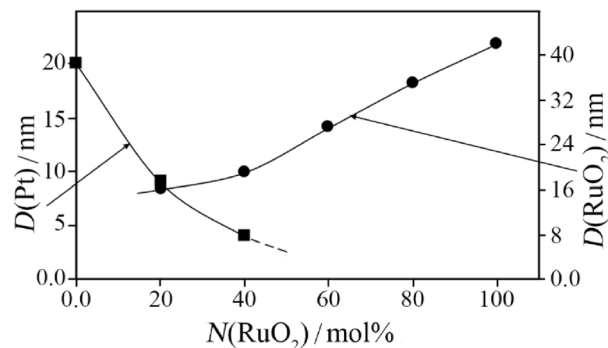

Fig. 3 The mean size of nanocrystals of Pt and RuO$_2$: filled square: $D(\text{Pt})$ and filled circle: $D(\text{RuO}_2)$ as a function of the nominal coating composition ($N(\text{RuO}_2)$)

Table 1 Effect of the nominal coating composition on some characteristics of the catalyst

Nominal coating composition /mol%	$N(Pt)$	100	80	60	40	20	0
	$N(RuO_2)$	0	20	40	60	80	100
Experimental coating composition /mol%	$N_e(Pt)$	100	74	55	38	19	0
	$N_e(RuO_2)$	0	26	45	62	81	100
Relative geometric surface area of Pt /cm^2 cm^{-2}	$A_s(Pt)$	1.00	0.82	0.67	0.42	0.20	0.00
Electrochemically active surface area of Pt /m^2 g^{-1}	$A(Pt)$	0.42 ± 0.02	0.46 ± 0.04	0.51 ± 0.06	0.46 ± 0.07	0.44 ± 0.10	0.00 ± 0.00
Mean nanocrystal size /nm	$D(Pt)$	20	9	4	<3	<3	0
	$D(RuO_2)$	0	16	19	27	35	42
Stationary current density of oxidation of propanol at -0.15 V /mA cm^{-2}	J_s	5.5	11.5	27	44	14	
	$J_{s,Pt}$	5.5	14	41	104	106	

of some other irregularities in the normal lattice arrangement, resulting from a nonstoichiometric composition [48, 49]. Residual chlorine increases both the microstrains and density of chaotically distributed dislocations in the crystal lattice. The catalytic activity of the Pt–RuO$_2$ catalyst, which are employed in the electrooxidation of simple organic molecules, is considerably influenced by these changes [36–38].

The catalytic activity of the mixture of Pt and RuO$_2$ nanocrystals, used for the oxidation of small organic molecules, depends on their microstructural and surface properties. The desired properties can be obtained by an adequate choice of process parameters of the catalyst formation (the nature of solvent, the nature of salts of Pt and Ru and their molar ratio in the solution applied on the Ti substrate, temperature and time of the electrode heating etc.). Table 1 represents the short summary of the most important microstructural and surface properties of the mixture of Pt and RuO$_2$ nanocrystals, dependable on the nominal content, and the effect of these properties on the catalytic activity in the oxidation of 1-propanol.

The effect of the chemical composition and microstructure of the Pt/RuO$_2$ coatings on their catalytic activity in the oxidation of 1-propanol in the alkaline environment was examined by recording cyclic voltammograms, chronoamperometric and polarization curves. The cyclic voltammograms of the oxidation of 1-propanol at the thermally prepared coatings composed of 100 mol% Pt or 20 mol% Pt and 80 mol% RuO$_2$ are presented in Figs. 4 and 5.

Figures 4 and 5 show that the onset potential of the 1-propanol oxidation at 20 mol% Pt, 80 mol% RuO$_2$ is approximately 40 mV more negative that the onset potential of the same reaction at 100 mol% Pt. The current density per relative geometric surface area of Pt, $j_{s,Pt}$, of the oxidation of 1-propanol at 20 mol% Pt, 80 mol% RuO$_2$ is 6.5 times higher than the current density at 100 mol% Pt. The catalytic activity of the Pt/RuO$_2$ coatings was also examined by recording the polarization curves. Figure 6 shows the polarization curves of the Pt/RuO$_2$ coatings with different chemical compositions. In the potential region from -0.36 to -0.08 V,
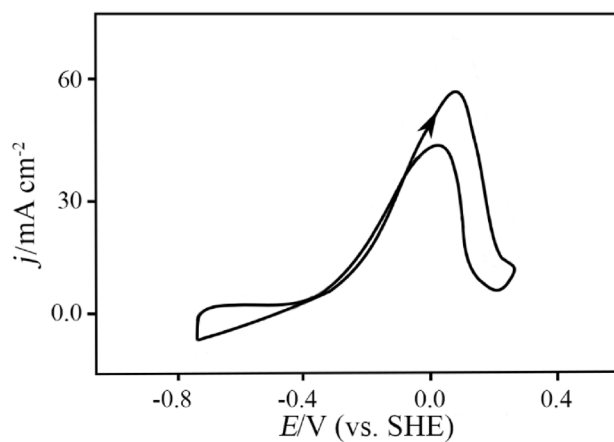
Fig. 4 Cyclic voltammograms of the oxidation of 1-propanol at 100 mol% Pt. Sweep rate 100 mV s^{-1} (1.0 mol dm^{-3} NaOH and 1.0 mol dm^{-3} 1-propanol, $t=25$ °C)
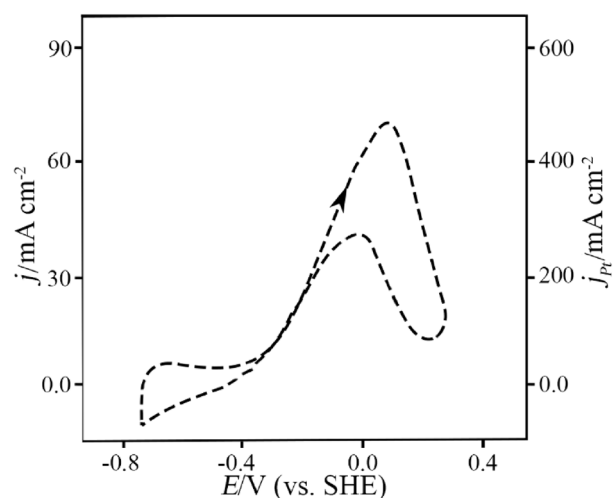
Fig. 5 Cyclic voltammograms of the oxidation of 1-propanol at 20 mol% Pt, 80 mol% RuO$_2$. Sweep rate 100 mV s^{-1} (1.0 mol dm^{-3} NaOH and 1.0 mol dm^{-3} 1-propanol)
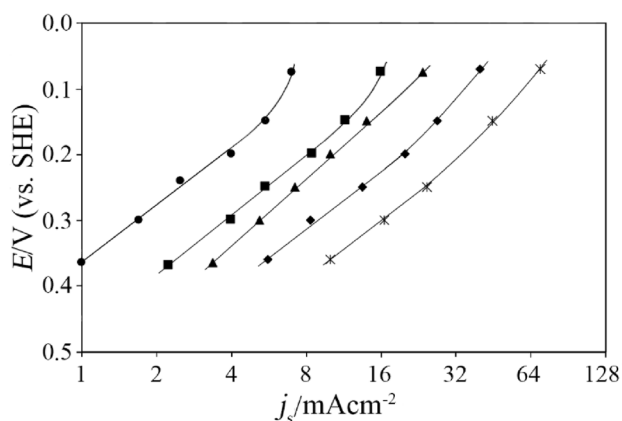
Fig. 6 Polarization curves of the oxidation of 1-propanol at the Pt/RuO$_2$ electrodes with different compositions: filled circle: 100 mol% Pt and filled triangle: 20 mol% Pt, 80 mol% RuO$_2$, star: 40 mol% Pt, 60 mol% RuO$_2$, filled diamond: 60 mol% Pt, 40 mol% RuO$_2$ and filled square: 80 mol% Pt, 20 mol% RuO$_2$. (1.0 mol dm^{-3} NaOH, 1.0 mol dm^{-3} 1-propanol, $t = 25$ °C)

the coating composed of 40 mol% Pt, 60 mol% RuO$_2$ shows the highest catalytic activity, as seen in Fig. 6. The effect of the chemical composition of the Pt/RuO$_2$ electrodes on their catalytic activity in the oxidation of 1-propanol is presented in Fig. 7 through the diagrams showing the dependence of j_s and $j_{s,Pt}$ on the RuO$_2$ content.

An increase in the RuO$_2$ content until 60 mol% results in the increase of the current density per unit geometric surface area, j_s. At this RuO$_2$ content, j_s reaches the maximum
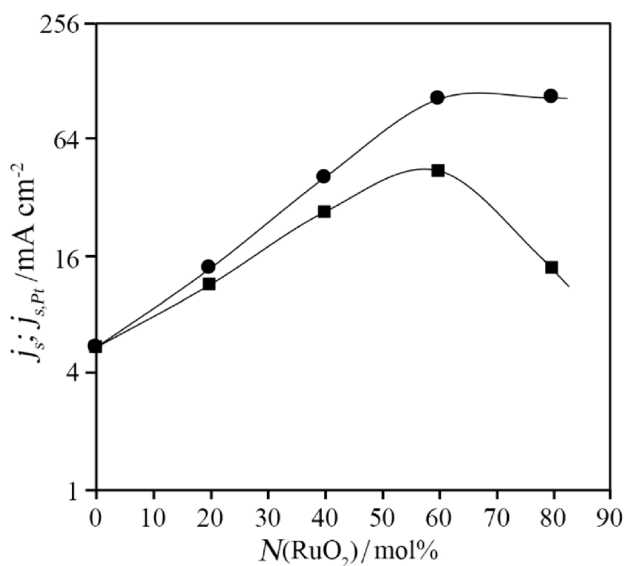

Fig. 7 Dependence of the stationary current densities, filled square: j_s and filed circle: $j_{s,Pt}$, on the coating composition in the oxidation of 1-propanol at -0.15 V (1.0 mol dm^{-3} NaOH, 1.0 mol dm^{-3} 1-propanol, $t = 25$ °C)

value. With increasing the RuO$_2$ content above 60 mol%, j_s decreases. Moreover, the increase in the RuO$_2$ content until 60 mol% results in slightly faster increase in the current density per relative surface area of Pt, $j_{s,Pt}$. However, the increase in the RuO$_2$ content above 60 mol% does not substantially affect $j_{s,Pt}$.

Chronoamperometric measurements were performed to examine the nature of the catalytic effect of Pt–RuO$_2$ electrodes in the oxidation of 1-propanol. During the potential shift to the anodic side, after the third cycle, the potential was held at the given value, E_h and simultaneously, the chronoamperometric curve was recorded. The obtained diagram is shown in Fig. 8.

The stationary state at the electrodes is achieved in about 22 min, as shown by the chronoamperometric curves. This state is associated with the stationary current density, j_s and stationary degree of coverage of the electrode surface with the adsorbed intermediates. The chronoamperometric curves also show that the increase in the RuO$_2$ content causes the slower decrease and lower overall reduction of the initial current densities. As a consequence, the equilibrium coverage degree of the surface of Pt nanocrystals with firmly adsorbed intermediates decreases with increasing the RuO$_2$ content [39].

The mechanism of the 1-propanol oxidation consists of several parallel and consecutive reactions as presented in Scheme 1 [7–9].

Propanal is formed in the primary reaction pathway at metallic Pt. Other oxidation reaction pathways are substantially slower with main products resulting from these pathways propionic acid and CO$_2$ [7–9]. The intermediates such as CO$_{ad}$, C$_2$H$_{yad}$, and CH$_{xad}$ are also formed by the secondary reaction pathways. They are firmly adsorbed on Pt [7–10]. The intermediates are stable at intermediate
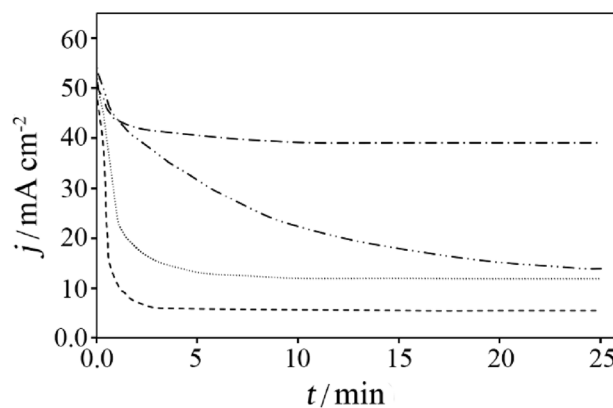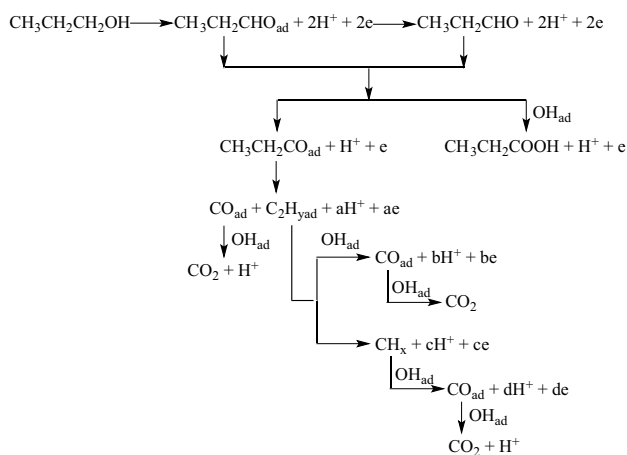

Fig. 8 Chronoamperometric curves of the oxidation of 1-propanol at -0.15 V, at (- - -) 100 mol% Pt; (• • • •) 80 mol% Pt, 20 mol% RuO$_2$; (−•−) 60 mol% Pt, 40 mol% RuO$_2$; (−••−) 20 mol% Pt, 80 mol% RuO$_2$, (1.0 mol dm^{-3} NaOH, 1.0 mol dm^{-3} 1-propanol, $t = 25$ °C)

Scheme 1

$$CH_3CH_2CH_2OH \longrightarrow CH_3CH_2CHO_{ad} + 2H^+ + 2e \longrightarrow CH_3CH_2CHO + 2H^+ + 2e$$

$$CH_3CH_2CO_{ad} + H^+ + e \qquad \qquad CH_3CH_2COOH + H^+ + e$$

$$\overset{OH_{ad}}{\longrightarrow}$$

$$CO_{ad} + C_2H_{yad} + aH^+ + ae$$

$$\overset{OH_{ad}}{\downarrow} \qquad \overset{OH_{ad}}{\longrightarrow} CO_{ad} + bH^+ + be$$

$$CO_2 + H^+ \qquad \overset{OH_{ad}}{\longrightarrow} CO_2$$

$$\longrightarrow CH_x + cH^+ + ce$$

$$\overset{OH_{ad}}{\longrightarrow} CO_{ad} + dH^+ + de$$

$$\overset{OH_{ad}}{\downarrow}$$

$$CO_2 + H^+$$

potentials, they slowly oxidize at higher potentials and form CO_2 [7–9]. Therefore, the intermediates block the Pt atoms at intermediate potentials and, thus, prevent the adsorption and dehydrogenation of subsequent molecules of 1-propanol on the Pt atoms. On the surface of the catalyst composed of the mixture of Pt and RuO_2 nanocrystals, OH_{ad} species are formed on the surface Ru atoms at potentials more negative than on Pt. These species oxidize at the border of the RuO_2 nanocrystals the firmly bound intermediates, positioned on adjacent Pt atoms. The final product of this oxidation is CO_2. The increased evolution of CO_2 is confirmed by the presence of the carbonate ions in the solution. Thus, the oxidized intermediates are released from the Pt atoms, leaving them ready to adsorb and dehydrogenate the subsequent molecules of 1-propanol [11–18, 23, 25, 29, 33–47]. The rapid oxidation of the firmly bound intermediates causes a lower equilibrium coverage of the Pt surface with the intermediates [39].

The rate of the electrooxidation of 1-propanol depends on the chemical composition of the catalyst (Figs. 6 and 7). The rate of oxidation per a relative geometric surface area of Pt ($j_{s,Pt}$) increases with increasing the rate of transfer of OH_{ad} species to the firmly bound intermediates. The amount of conveyed OH species increases when the specific length (the length per unit surface area of the Pt nanocrystal) of the border between nanocrystals of Pt and RuO_2 increases. The increase in the RuO_2 content affects both directly and indirectly the increase of the specific border length. The direct effect is a consequence of the increased number of RuO_2 nanocrystals, whereas the indirect effect results from the decrease in the average size of Pt nanocrystals (Fig. 3).

The decrease in the average size of Pt nanocrystals causes the increase in the density of chaotically distributed dislocations and inner microstrains [57–59]. These changes increase the steric hindrance in the adsorption of intermediates, resulting in the decrease in the strength of the adsorption

bonds [23]. Weaker bonds cause the faster oxidation of intermediates and a lower coverage degree of Pt with the intermediates [23]. The increase in the rate of oxidation of 1-propanol per geometric surface area of Pt, with increasing the RuO_2 content is presented in Fig. 7 through the dependence of $j_{s,Pt}$ on the RuO_2 content. The diagrams in Figs. 3 and 7 show that the increase in the RuO_2 content until 50 mol% causes the linear increase of $j_{s,Pt}$. Further increase in the RuO_2 content results in inconsiderable increase of $j_{s,Pt}$. To achieve the adsorption and dehydrogenation of 1-propanol on Pt nanocrystals, an assemble containing several free adjacent Pt atoms is necessary. This assemble is needed since the adsorbed species $CH_3CH_2CHO_{ad}$ attach to Pt nanocrystals via adsorption bonds. This is achieved by binding three C atoms of propanol to three adjacent surface Pt atoms. Plausibly, interactions between Pt atoms and oxygen atoms are also established. As a result of dehydrogenation of propanol in the first stage, the hydrogen atoms, adsorbed on Pt, are probably formed. These atoms subsequently desorb and form $H^+ + e$ species. Therefore, the assembles of six free, adjacent Pt atoms, adequately positioned, are required to provide the maximum rate of formation of $CH_3CH_2CHO_{ad}$ species. With decreasing the size of nanocrystals until 4 nm, the number of these assemblies per unit surface area of Pt slightly decreases [60]. Therefore, the effect of the decrease in the number of assemblies of adjacent Pt atoms on $j_{s,Pt}$ is neglected at the electrodes with less than 56% of RuO_2. When considering these electrodes, the dominant effect which causes the increase of $j_{s,Pt}$ with increasing the RuO_2 content is the increase in the length of the border between crystal grains, the density of chaotically distributed dislocations and inner microstrains. However, with decreasing the average size of nanocrystals below 4 nm, the number of assemblies of adjacent Pt atoms required for the adsorption and dehydrogenation of 1-propanol sharply decreases [60]. The decrease in the number of these assemblies results in the decrease in the rate of 1-propanol oxidation, which almost completely cancels the rate increase caused by the increase in the length of the border between crystal grains (Fig. 7).

The stationary density j_s (the density per geometric surface area) increases slower than $j_{s,Pt}$ with increasing the RuO_2 content until the maximum value. This is a consequence of the decrease in the contribution of the Pt surface in the geometric surface area of the Pt/RuO_2 electrodes. After reaching the maximum value, j_s declines relatively rapidly. This decrement is caused by the decrease in the number of assemblies of adjacent Pt atoms, necessary for the adsorption and dehydrogenation of 1-propanol as a consequence of (a) the decrease in the contribution of the Pt surface to the geometric surface area of the Pt/RuO_2 electrodes; (b) the decrease in the average size of nanocrystals. The maximum value of j_s is obtained at the optimal content of the Pt/RuO_2 electrodes. These electrodes show the optimal

relation between the length of the contact edge and number of assemblies of adjacent Pt atoms.

Considering the experimental results and theoretical analysis, the correlation between the microstructure and catalytic activity was determined, as well as the optimal content of the Pt/RuO$_2$ catalysts, used in the electrochemical oxidation of 1-propanol in the alkaline environment. Future studies should be directed towards determination of the catalytic effect and stability of these catalysts, applied on various highly porous substrates.

Conclusion

The thermal procedure was used to prepare the catalyst, composed of the mixture of nanocrystals of metallic Pt and rutile Ru, on the titanium substrate. The catalyst composition affects its microstructure, surface properties and catalytic activity in the electrochemical oxidation of 1-propanol in the alkaline environment. The mixture composition determines the average size of Pt and RuO$_2$ nanocrystals, length of the contact edges between the Pt and RuO$_2$ nanocrystals, density of chaotically distributed dislocations, inner microstrains, real surface area of the catalyst, contribution of the Pt surface to the entire surface and number of assemblies of adjacent Pt atoms at the Pt surface, required for the adsorption of 1-propanol. A correlation between the microstructure and surface properties, as well as the catalytic activity in the oxidation of 1-propanol was determined. The maximum catalytic activity showed the catalyst with the optimal ratio between the length of the contact edge and number of assemblies of adjacent Pt atoms. The catalytic effect is a result of the bifunctional mechanism of the mixture of Pt and RuO$_2$ nanocrystals. The Ru-OH species are formed on Ru atoms, at potentials more negative than on Pt. These species oxidize the firmly adsorbed intermediates, propionyl, CO$_{ad}$, C$_2$H$_{yad}$, and CH$_{xad}$ and, thus, release the Pt atoms for the adsorption and dehydrogenation of the subsequent molecules of propanol.

Experimental

To activate a titanium substrate (plates with a surface area of 3.0 cm^2) for the electrochemical oxidation of 1-propanol, the mixture of nanocrystals of RuO$_2$ and metallic Pt was thermally prepared on the substrate, as previously described [36]. First, the titanium plates were roughed and subsequently, cleaned with ethanol saturated with sodium hydroxide at 25 °C. The plates were rinsed with distilled water and then kept for about 5 min in boiling 20 wt% HCl. Finally, after thorough rinsing with distilled water, the titanium plates were dried in hot air. The solutions of H$_2$PtCl$_6$ and RuCl$_3$ (Johnson and Matthey) in 2-propanol (the concentration of 10 mg cm^{-3} based on the pure metals) were spread over the prepared plates. To obtain the desired composition of the coating, the ratio H$_2$PtCl$_6$:RuCl$_3$ in the solution was varied. After evaporation of the solvent, the electrodes were heated at 500 °C in the air atmosphere. This procedure was repeated five times until the coating depth of 1.2 g m^{-2} based on the pure metals was achieved. In the final step, the last layer was applied and the electrodes were heated for 45 min at 500 °C.

An electronic dispersion spectroscopy, EDS (QX3000 spectrometer) was used to determine the average chemical composition of the layer.

A Phillips PW1730 diffractometer equipped with a PW 1050 vertical goniometer and static non-rotating sample carriers was used for X-ray diffraction analyses. A power supply of 35 kV, 20 mA for copper excitation and an AMR graphite monochromator were used. Phases were identified by reference to ASTM tables. The mean nanocrystallite sizes, D(Pt) and D(RuO$_2$), were determined from the full width at half maximum (β) by Scherrer's formula $D = 0.94 \lambda/(\beta \cos\theta)$.

The electrical set-up composed of a potentiostat equipped with a programmer (Potentiostat–Galvanostat model 173, EGG Princeton, Applied Research, Princeton, USA), X–Y recorder (Hewlett Packard 7035 B) and digital voltmeter (Pros Kit 03–9303 C) was used for the electrochemical measurements. A standard electrochemical cell with a separate compartment for a saturated calomel electrode and a Luggin capillary was used for the experiments. Platinum was the counter electrode. It was a flat-mesh shaped with a geometric surface area of 16 cm^2 and positioned parallel to the working electrode. A thermostat was set at operating temperature of 25 ± 0.5 °C and the electrochemical cell was placed into it. All solutions were prepared from p.a. chemicals (Merck) and demineralized water. Before all electrochemical measurements, the solution was liberated from oxygen by its replacement with nitrogen. Prior to use, nitrogen was purified by passing over molecular sieves and copper shavings. The potentials were expressed relative to the standard hydrogen electrode. The potentials of polarization curves were corrected for the ohmic drop, determined by the galvanostatic pulse method. The current density was recorded after holding the electrode for 25 min at the desired potentials. Stationary current densities (the current per unit geometric surface area, j_s and the current per relative geometric surface area of Pt in the alloy Pt–RuO$_2$, $j_{s,Pt}$) were determined. $j_{s,Pt}$ was calculated from the equation $j_{s,Pt} = j_s \frac{Q(H)_{Pt-RuO_2}}{Q(H)_{Pt}}$, where $Q(H)_{Pt-RuO_2}$ refers to the charge of hydrogen desorption of the Pt–RuO$_2$ electrodes and $Q(H)$ is the charge of hydrogen desorption of 100 mol% Pt electrode.

References

1. Nacef M, Chelaghmia ML, Affoune AM, Pontié M (2019) Mater Res Found 49:103
2. Barragán VM, Heinzel A (2002) J Power Sources 104:66
3. Tang H, Wang S, Pan M, Jiang SP, Ruan Y (2007) Electrochim Acta 52:3714
4. Sumodjo PTA, da Silva EJ, Rabockai T (1989) J Electroanal Chem Interf Electrochem 271:305
5. Jusys Z, Behm RJ (2009) Methanol, formaldehyde, and formic acid adsorption/oxidation on a carbon-supported Pt nanoparticle fuel cell catalyst: a comparative quantitative DEMS study. In: Koper MTM (ed) Fuel cell catalysis: a surface science approach, Chapter 13. Wiley, Hoboken, New Jersey, p 411
6. Heinen M, Jusys Z, Behm RJ (2009) Handbook of fuel cells, Chapter 12. Wiley, Chichester, p 183
7. Schnaidt J, Jusys Z, Behm RJ (2012) J Phys Chem C 116:25852
8. Schnaidt J, Heinen M, Jusys Z, Behm RJ (2013) Electrochim Acta 104:505
9. Pastor E, Wasmus S, Iwasita T, Arévalo MC, Gonzalez S, Arvia AJ (1993) J Electroanal Chem 350:97
10. Kutz RB, Braunschweig B, Mukherjee P, Behrens RL, Dlott DD, Wieckowski A (2011) J Catal 278:181
11. Liu J, Ye J, Xu C, Jiang SP, Tong Y (2008) J Power Sources 177:67
12. Wang B, Tao L, Cheng Y, Yang F, Jin Y, Zhou C, Yu H, Yang Y (2019) Catalysts 9:387
13. Sun S, Sun L, Xi S, Du Y, Prathap MUA, Wang Z, Zhang Q, Fisher A, Xu ZJ (2017) Electrochim Acta 228:183
14. Wang D, Liu J, Wu Z, Zhang J, Su Y, Liu Z, Xu C (2009) Int J Electrochem Sci 4:1672
15. Zalineeva A, Serov A, Padilla M, Martinez U, Artyushkova K, Baranton S, Coutanceau C, Atanassov P (2015) Electrochem Commun 57:48
16. Okanishi T, Katayama Y, Ito R, Muroyama H, Matsui T, Eguchi K (2016) Phys Chem Chem Phys 18:10109
17. Ye J, Liu J, Xu C, Jiang SP, Tong Y (2007) Electrochem Commun 9:2760
18. Antolini E, Gonzalez ER (2010) J Power Sources 195:3431
19. Wang Y, Li L, Hu L, Zhuang L, Lu J, Xu B (2003) Electrochem Commun 5:662
20. Matsuoka K, Iriyama Y, Abe T, Matsuoka M, Ogumi Z (2005) J Power Sources 150:27
21. Varcoe JR, Slade RCT, Yee ELH (2006) Chem Commun 13:1428
22. Modestov AD, Tarasevich MR, Pu H (2016) Electrocatalysis 7:42
23. de Rodrigues A, De Souza JPI, Pastor E, Nart FC (1997) Langmuir 13:6829
24. González-Cobos J, Baranton S, Coutanceau C (2016) J Phys Chem C 120:7155
25. Rodrigues IA, Bergamaski K, Nart FC (2003) J Electrochem Soc 150:E-89
26. Tran K, Nguyen TQ, Bartrom AM, Sadiki A, Haan JL (2014) Fuel Cells 14:834
27. Shen PK, Xu C (2006) Electrochem Commun 8:184
28. Bott-Neto JL, Garcia AC, Oliveira VL, de Souza NE, Tremiliosi-Filho G (2014) J Electroanal Chem 735:57
29. Chu YH, Shul YG (2010) Int J Hydrog Energy 35:11261
30. Zhang Y, Yi Q, Chu H, Nie H (2017) J Fuel Chem Tech 45:475
31. Jafarian M, Rashvand Avei M, Gobal F, Rayati S, Mahjani MG (2011) Electrocatalysis 2:163
32. Tamiji T, Nezamzadeh-Ejhieh A (2019) Solid State Sci 98:106033
33. Rigsby MA, Zhou W-P, Lewera A, Duong HT, Bagus PS, Jaegermann W, Hunger R, Wieckowski A (2008) J Phys Chem C 112:15595
34. Long JW, Stroud RM, Swider-Lyons KE, Rolison DR (2000) J Phys Chem B 104:9772
35. Watanabe M, Motoo S (1975) J Electroanal Chem Interf Electrochem 60:267
36. Spasojević M, Ribić-Zelenović L, Spasojević M, Marković D (2020) Russ J Electrochem 56:1208
37. Spasojevic M, Spasojevic M, Ribic-Zelenovic L (2020) Monatsh Chem 151:33
38. Spasojević M, Ribić-Zelenović L, Spasojević M, Trišović T (2019) Russ J Electrochem 55:1350
39. Spasojević M, Ribic-Zelenović L, Spasojević M, Trišović T (2020) Rev Roum Chim 65:481
40. Spasojevic M, Spasojevic M, Ribic-Zelenovic L, Markovic D (2021). Z Phys Chem. https://doi.org/10.1515/zpch-2020-1794
41. Wakisaka M, Mitsui S, Hirose Y, Kawashima K, Uchida H, Watanabe M (2006) J Phys Chem B 110:23489
42. Waszczuk P, Lu G-Q, Wieckowski A, Lu C, Rice C, Masel RI (2002) Electrochim Acta 47:3637
43. Lu C, Rice C, Masel RI, Babu PK, Waszczuk P, Kim HS, Oldfield E, Wieckowski A (2002) J Phys Chem B 106:9581
44. Liu H, Song C, Zhang L, Zhang J, Wang H, Wilkinson DP (2006) J Power Sources 155:95
45. Zhao X, Yin M, Ma L, Liang L, Liu C, Liao J, Lu T, Xing W (2011) Energy Environ Sci 4:2736
46. Kakati N, Maiti J, Lee SH, Jee SH, Viswanathan B, Yoon YS (2014) Chem Rev 114:12397
47. Tian T, Shi S, Shen Y, Yin H (2019) Electrochim Acta 293:390
48. Spasojević MD, Krstajić NV, Jakšić MM (1987) J Mol Catal 40:311
49. Spasojević M, Ribić-Zelenović L, Spasojević P (2012) Ceram Int 38:5827
50. Galizzioli D, Tantardini F, Trasatti S (1975) J Appl Electrochem 5:203
51. Burke LD, O'Neill JF (1979) J Electroanal Chem Interf Electrochem 101:341
52. Franaszczuk K, Sobkowski J (1992) J Electroanal Chem 327:235
53. Profeti LPR, Profeti D, Olivi P (2009) Int J Hydrog Energy 34:2747
54. Comninellis C, Vercesi GP (1991) J Appl Electrochem 21:136
55. Comninellis C, Vercesi GP (1991) J Appl Electrochem 21:335
56. Hu C-C, Lee C-H, Wen T-C (1996) J Appl Electrochem 26:72
57. Ćirović N, Spasojević P, Ribić-Zelenović L, Mašković P, Spasojević M (2015) Sci Sintering 47:347
58. Ribić-Zelenović L, Spasojević M, Maričić A, Ristić MM (2009) Sci Sintering 41:175
59. Spasojević M, Ćirović N, Ribić-Zelenović L, Spasojević P, Maričić A (2014) J Electrochem Soc 161:D463
60. Park I-S, Lee K-S, Choi J-H, Park H-Y, Sung Y-E (2007) J Phys Chem C 111:19126